

# Optics Letters

## Magnetometry using fluorescence of sodium vapor

TINGWEI FAN,<sup>1,2</sup> LEI ZHANG,<sup>1</sup> XUEZONG YANG,<sup>1,2</sup> SHUZHEN CUI,<sup>1</sup> TIANHUA ZHOU,<sup>1,3</sup>  AND YAN FENG<sup>1,\*</sup> 

<sup>1</sup>Shanghai Key Laboratory of Solid State Laser and Application, and Shanghai Institute of Optics and Fine Mechanics, Chinese Academy of Sciences, Shanghai 201800, China

<sup>2</sup>University of the Chinese Academy of Sciences, Beijing 100049, China

<sup>3</sup>e-mail: siomzth@mail.siom.ac.cn

\*Corresponding author: feng@siom.ac.cn

Received 20 September 2017; revised 14 November 2017; accepted 21 November 2017; posted 22 November 2017 (Doc. ID 307515); published 19 December 2017

**Magnetic resonance of sodium fluorescence is studied with varying laser intensity, duty cycle, and field strength. A magnetometer based on a sodium vapor cell filled with He buffer gas is demonstrated, using a single amplitude-modulated laser beam. With a 589 nm laser tuned at the  $D_1$  or  $D_2$  line, the magnetic field is inferred from the variation of fluorescence. A magnetic field sensitivity of  $150 \text{ pT}/\sqrt{\text{Hz}}$  is achieved at the  $D_1$  line. The work is an important step toward sensitive remote magnetometry with mesospheric sodium.** © 2017 Optical Society of America

**OCIS codes:** (020.1335) Atom optics; (020.7490) Zeeman effect; (300.6280) Spectroscopy, fluorescence and luminescence; (280.4788) Optical sensing and sensors.

<https://doi.org/10.1364/OL.43.000001>

In the past two decades, atomic magnetometer research has made significant advances. The sensitivity of atomic magnetometers rivals [1,2] and even surpasses [3,4] that of superconducting quantum interference device (SQUID)-based magnetometers. A magnetometer based on vapor of alkali atoms (Rb, Cs, or K) has been a research focus [5–7]. Sodium atoms were initially used in various spectral studies [8–10]. However, magnetometer using sodium atom had not been investigated because of its relatively low vapor pressure and lack of suitable pump laser source.

In 2011, Higbie *et al.* proposed a method for remotely measuring the geomagnetic field by interrogating sodium atoms in the mesosphere with a pulsed laser at the sodium resonance wavelength [11]. Measurement of magnetic field on the 100 km length scale is significant for many geophysical applications including mapping of crustal magnetism and ocean circulation measurements. Kane *et al.* demonstrated an initial measurement based on mesospheric sodium in 2016. A measurement sensitivity of  $162 \text{ nT}/\sqrt{\text{Hz}}$  was reported [12]. Considering the complexity and cost, experimental study in the lab is beneficial before the on-sky test. Under laboratory condition, it is easier to make a subtle investigation with higher

sensitivity. Indeed, it is difficult to mimic the physical condition of the mesospheric sodium layer in the lab. But the same quantum law governs the light and sodium atom interaction either in 90 km high altitude or in a vapor cell on the ground. Laboratory study of sodium magnetometry is a necessary step toward the realization of high sensitivity remote magnetometry with mesospheric sodium.

In this Letter, we present a study on the magnetic resonance of sodium fluorescence and a demonstration of a sodium magnetometer. Considering the feasibility in extending the scheme to mesospheric sodium later, fluorescence signal from a sodium vapor cell is used for the measurement. Buffer gas is filled to increase the spin polarization lifetime by slowing the diffusion of atomic sodium to the cell walls. The magnetometer, which uses a single amplitude-modulated laser beam, is a Bell–Bloom type [13]. By modulating the laser amplitude around the Larmor frequency, a magnetic resonance happens because of the coherence reinforced by synchronizing optical pumping with the spin precession. A magnetic field sensitivity of  $150 \text{ pT}/\sqrt{\text{Hz}}$  is achieved at the Na  $D_1$  line.

The schematic diagram of the experimental setup is shown in Fig. 1. The light source is a frequency-doubled diode-seeded

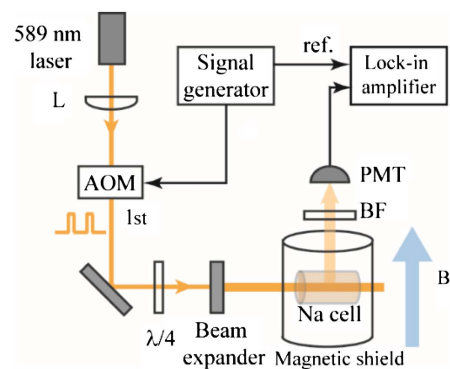


**Fig. 1.** Schematic of the experimental arrangement for a sodium magnetometer with amplitude modulation. L, lens;  $\lambda/4$ , quarter-wave plate; PMT, photomultiplier tube; BF, bandpass filter.

Raman fiber amplifier, which provides up to a 1 W continuous wave 589 nm laser with a measured linewidth of  $\sim 5$  MHz (similar to the one reported in Ref. [14]). A wavelength meter is used to monitor and control the center wavelength of the laser in real time, with an absolute accuracy of 200 MHz. After collimation, the linearly polarized laser is amplitude modulated by an acousto-optic modulator (AOM). The first-order diffraction is chosen to work with because of the higher extinction ratio than the zero order. A quarter-wave plate changes the laser from linear to circular polarization. The laser beam is expanded to 3.7 mm in diameter and then illuminates the cylindrical sodium vapor cell whose radius and length are 1.5 cm and 5 cm, respectively. The sodium vapor cell contains Na with 100 torr He buffer gas, which was heated to 60°C by channeling warm air into the cell oven. The cell oven is inside a four-layer magnetic shield that provides nearly isotropic shielding of external magnetic fields. An adjustable magnetic field is generated along the axial direction of the cylindrical magnetic shield with a magnetic coil. In the experiments, the laser beam direction is perpendicular to the magnetic field at the vapor cell.

The fluorescence of the sodium vapor is detected through an axial hole of the magnetic shield. In the magnetic resonance study, a photon counting head (Hamamatsu H10682-210) is used with a photon counter (Hamamatsu C8855-01). A 589 nm filter with a full width at half maximum (FWHM) linewidth of 1 nm (Alluxa 589.45-1 OD6 ULTRA Bandpass Filter) is put before the detector to reduce the background light. Alternatively, a photomultiplier tube (Hamamatsu R9880U-210) and lock-in amplifier (Stanford Research Systems SR830) are used to measure the magnetic field and analyze the measurement sensitivity. A modulated pulse signal is applied to drive the AOM, and the sync output of the signal generator acts as the reference signal of the lock-in amplifier. The lock-in amplifier demodulates the experimental signal at the reference frequency.

The sodium fluorescence is measured in the direction perpendicular to the laser beam. Measuring at the backward direction is more consistent with the expected setup of remote magnetometry with mesospheric sodium. However, trouble with backscattered stray light was encountered in the experiments. The perpendicular direction was chosen instead for less stray light. Special attention was paid to decrease the background illumination of the photon detector from the scattered radiation of the laser.

Because of the dark magnetic resonance and correspondingly reduced photon shot noise, the  $D_1$  line is expected to allow better sensitivity [11]. The laser was therefore tuned to the sodium  $D_1$  line (589.7558 nm). The sodium atom density is low at room temperature ( $7.89 \times 10^5$  atoms/cm<sup>3</sup> at 25°C [15]). At the temperature of 60°C, the sodium density is approximately  $6.65 \times 10^7$  atoms/cm<sup>3</sup>. The spin relaxation time is calculated to be 48 ms (considering the 60°C temperature, the 100 torr He buffer gas, and the cell dimension [16,17]). The FWHM width of the sodium  $D_1$  line is measured to be 2.8 GHz at the experimental condition. The spectral line is collision broadened strongly such that the hyperfine structure is blurred. In the experiments, the best results are obtained with the laser tuned at 589.7558 nm, which is the transition wavelength between fine energy levels  $3^2S_{1/2}$  and  $3^2P_{1/2}$ .

Rectangular pulse signals are applied to the AOM which produces an amplitude modulated laser. The repetition

frequency is scanned across the Larmor frequency. The fluorescence photons are counted synchronously with the pulse repetition frequency scan. Magnetic resonance lines were recorded for different duty cycle and peak intensity of the laser, and varying magnetic field. A typical resonance line is shown in Fig. 2. The lineshape is close to Lorentzian. For the magnetic resonance shown in Fig. 2, the Larmor frequency  $\nu_L$  and the FWHM of magnetic resonance  $\Delta f$  are 297.17 kHz and 580 Hz, respectively. The magnetic field  $B$  is  $\nu_L/g = 42460$  nT, where  $g = 6.99812$  Hz/nT is the gyromagnetic ratio of atomic sodium. The shot-noise-limited (SN-limited) sensitivity is calculated to be 147 pT/ $\sqrt{\text{Hz}}$  with the formula [11]

$$\delta B_{\text{SN}} = 4\sqrt{3}\Delta f/9g \times \left( \sqrt{R_{\text{Dip}} + R_{\text{Back}}} \right) / (|R_{\text{Dip}} - R_{\text{Back}}|), \quad (1)$$

where  $R_{\text{Dip}}$  and  $R_{\text{Back}}$  are the photon detection rates ( $R_{\text{det}}$ ) at resonance and background, respectively. The formula is valid for the case that the resonance shape is Lorentzian. It is used to quickly assess the magnetic resonance signal and find the optimum condition for sensitive magnetic field measurement.

Figure 3 shows plots of magnetic resonance width ( $\Delta f$ ), resonance height ( $h$ ), and calculated SN-limited sensitivity ( $\delta B$ ) as functions of laser peak intensity and pulse duty cycle. In these experiments, the magnetic field is fixed at 42460 nT. When varying the laser peak intensity as in Fig. 3(a), the pulse duty cycle is fixed at 20%. It is found that the magnetic resonance width increases linearly with the increase of the peak intensity. The relative resonance height is saturated at high peak

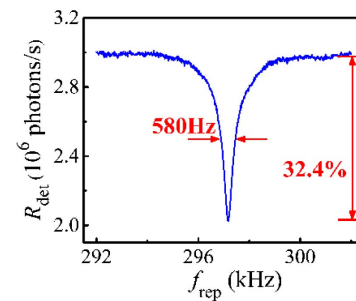


**Fig. 2.** Typical magnetic resonance signal of Na  $D_1$  line, where the peak laser intensity is  $65 \text{ W/m}^2$ , pulse duty cycle is 17.5%, and cell temperature is 60°C.

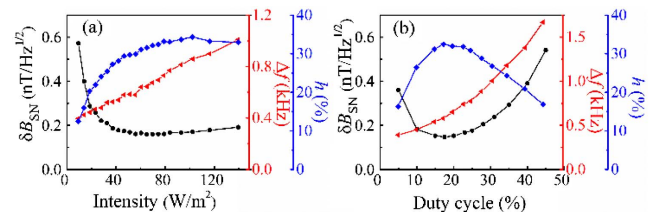


**Fig. 3.** Plots of magnetic resonance width ( $\Delta f$ ), relative resonance height ( $h$ ), and SN-limited sensitivity ( $\delta B_{\text{SN}}$ ) as functions of the laser peak intensity and pulse duty cycle. (a) Dependence on peak intensity at a pulse duty cycle of 20%. (b) Dependence on duty cycle at a fixed laser intensity of  $65 \text{ W/m}^2$ .

intensity. The highest SN-limited sensitivity is calculated at a laser intensity of  $65 \text{ W/m}^2$ . Then in the pulse duty cycle optimization in Fig. 3(b), the laser intensity is fixed at  $65 \text{ W/m}^2$ . The resonance width increases with the duty cycle. The resonance height depends on the duty cycle strongly and has an optimum around 17.5%. As a result, a close to optimum condition is determined at a duty cycle of 17.5% and peak intensity of  $65 \text{ W/m}^2$ . The respective resonant fluorescence signal is shown in Fig. 2 and discussed in previous paragraph.

The magnetic resonance not only happens at the Larmor frequency but also at the subharmonics of the Larmor frequency. While the resonance at the Larmor frequency corresponds to the physical case that the sodium atoms are excited at every Larmor period, the resonances at subharmonics correspond to excitation at every multiple Larmor periods. Figure 4(a) plots the multiple resonance signal when the laser duty cycle is 20%. Second and third subharmonics are clearly observed. More subharmonics can be observed with smaller duty cycle. The observation suggests that if the high-power high repetition rate 589 nm laser is not available, lasers with lower repetition rate can also be considered for remote magnetometry experiments, as long as the pulse period is much shorter than the spin polarization lifetime of the mesospheric sodium. Figure 4(b) plots the case when the magnetic field is 516 nT, much smaller than that in Fig. 4(a). It is found that the Larmor resonance and subharmonic resonance start to overlap with each other. At even a smaller magnetic field, the resonance width cannot be read accurately so that simple estimation of the SN-limited sensitivity with Eq. (1) is not feasible.

Figure 5(a) shows plots of magnetic resonance width, relative resonance height, and calculated SN-limited sensitivity as functions of the magnetic field, where the laser duty cycle is 20% and the peak intensity is  $65 \text{ W/m}^2$ . With decreasing

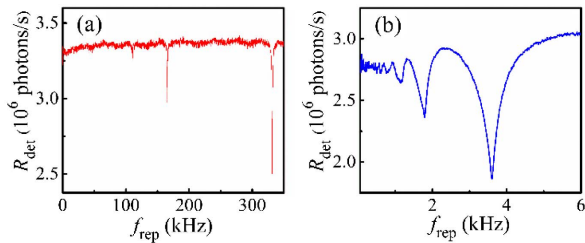


**Fig. 4.** Multiple magnetic resonance signal at a duty cycle of 20% and peak laser intensity of  $65 \text{ W/m}^2$ . (a) Magnetic field of 47,371 nT. (b) Magnetic field of 516 nT.

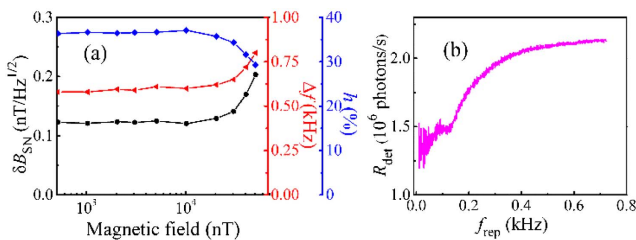


**Fig. 5.** (a) Magnetic field dependence of magnetic resonance width, relative resonance height, and calculated SN-limited sensitivity. (b) Magnetic resonance signal at a field strength of 18 nT, where the laser duty cycle is 20% and the peak intensity is  $65 \text{ W/m}^2$ .

magnetic field, the resonance width decreases, the resonance height increases, and so the SN-limited sensitivity improves. At lower magnetic field, the resonance width and relative height almost keep constant. The SN-limited sensitivity is about  $122 \text{ pT}/\sqrt{\text{Hz}}$ . For a magnetic field less than 500 nT, the resonance signal can still be clearly observed, although the Larmor resonance and subharmonic resonance overlap more. The resonance signal for a magnetic field as low as  $<20 \text{ nT}$  can be detected, as seen in Fig. 5(b). Therefore, the setup can be used to detect not only a geomagnetic field but also a small field. The minimum detectable field is determined by the spin relaxation time of sodium atoms. The spin relaxation time is estimated to be 48 ms in our experimental condition. To drive a coherence, the relaxation rate should be at least a few times lower than the spin-precession frequency, so a minimum detectable magnetic field of about 20 nT is reasonable.

To make a sensitive measurement of the magnetic field, we utilize a phase-sensitive technique [18]. The detector is switched to a photomultiplier tube with analog output. The laser pulse repetition frequency  $f_{\text{rep}}$  is modulated around a central frequency  $f_c$ :  $f_{\text{rep}} = f_c + f_{\text{dev}} \cos(2\pi f_{\text{mod}} t)$ , where  $f_{\text{mod}}$  is the modulation frequency and  $f_{\text{dev}}$  is the amplitude of modulation. The detected signal is demodulated with a lock-in amplifier referenced to the modulation frequency  $f_{\text{mod}}$ . The output of the lock-in amplifier is linear  $S_{\text{LI}} \approx \alpha(f_c - f_{\text{res}})$  as a function of  $f_c - f_{\text{res}}$  when  $|f_c - f_{\text{res}}| < \Delta f/2$ , where  $f_{\text{res}}$  is resonance frequency. The slope  $\alpha \propto l/\Delta f$  is extracted from the trace in Fig. 6(a), which shows dispersive shaped resonance from the X output of the lock-in amplifier, where  $l$  is the contrast of magnetic resonance. The slope  $\alpha$  depends on  $f_{\text{mod}}$ . The modulation frequency should be slow enough to allow adequate optical pumping. Meanwhile, the modulation frequency should be fast enough because of the bandwidth requirement and the increasing intensity noise at low frequency of the laser. We tested multiple modulation frequencies, and 500 Hz was chosen.

The lock-in signal is linear for small changes  $\Delta B$ , when the central repetition frequency is set to a certain value around  $f_{\text{res}}$ . Spectral dependence of the noise contributions is determined from a radio frequency analysis of the X output of the lock-in amplifier (Stanford Research SR785 Dynamic Signal Analyzer). The root-mean-square (rms) magnetic field fluctuations ( $S_B$ ) are shown in Fig. 6(b). For frequencies in the range of 1–100 Hz, a noise floor of  $150 \text{ pT}/\sqrt{\text{Hz}}$  is reached. For frequencies below 1 Hz, additional noise is present. Above 100 Hz the noise decreases due to the finite time constant

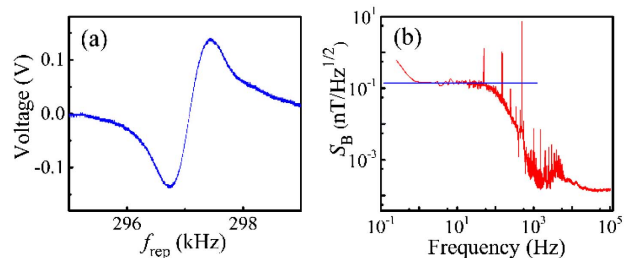


**Fig. 6.** Measurement of magnetic field with PMT and lock-in amplifier with a modulation frequency of 500 Hz. (a) Lock-in signal as a function of the central repetition frequency  $f_c$  that is scanned over a magnetic resonance. (b) Magnetic field noise spectrum.

of the lock-in amplifier (here 1 ms), which reduces the bandwidth to  $\sim 300$  Hz. Several noise peaks are also present; these are at the line frequency and its harmonics.

Several measures can be used to potentially reduce the noise floor or sensitivity. The beam spot size is only 3.7 mm right now. With bigger beam spot, the number of the interacting sodium atoms will increase. The optical setup for fluorescence detection can be improved for collecting more photons. Moreover, there are technical noise sources related to the power and wavelength stability of the pump laser. We are going to replace the laser with one of better power stability. The wavelength will be locked with Doppler-free saturated absorption spectroscopy, which will improve the wavelength stability greatly compared to the current wavemeter-based method.

We have demonstrated magnetometry with sodium vapor by detecting the fluorescence. Nevertheless, there is an observation we could not understand yet. There is a small dip on the high-frequency side of the magnetic resonance. This feature becomes obvious at lower laser power, where the resonance width decreases. When the laser intensity is low such that the resonance width is less than its spacing from the dip, the dip can be resolved. A typical resonance signal with the side feature is shown in Fig. 7(a). The frequency spacing between the dip and center frequency of the magnetic resonance is measured with respect to the magnetic field. A linear dependence is found as shown in Fig. 7(b).

Magnetic resonance of sodium fluorescence pumped at the  $D_2$  line (589.1583 nm) was investigated as well. While a peak signal was expected according to previous simulation [11], a valley was observed. The center frequency of the valley signal varies with the magnetic field, confirming that it is a magnetic resonance signal. We believe the observation is related to the direction of the fluorescence detection. At a good optical pumping condition, as is at the magnetic resonance, a majority of the sodium fluorescence is circularly polarized. The pattern of circular polarization emission is peanut-shaped [19]. Therefore, the emission to the perpendicular direction is actually reduced compared to off-resonance condition, resulting in a valley at the resonance. At off-resonance condition, the precession of sodium atoms in the magnetic field destroys the effect of optical pumping. The circular polarization fluorescence loses its majority. A direct confirmation would be a measurement at the backward direction; however, this cannot be achieved in our current setup.

In summary, we have investigated the magnetic resonance of sodium fluorescence and demonstrated a magnetometer based on a sodium vapor cell with He buffer gas for the first time, to the best of our knowledge. The setup can be used to measure a

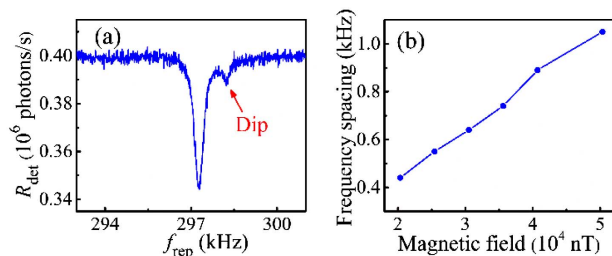


**Fig. 7.** (a) Typical resonance line at small light intensity for Na  $D_1$  line. (b) Frequency shift of the small dip relative to the resonance frequency as a function of magnetic field.

magnetic field ranging from  $\sim 20$  nT to the geomagnetic field and higher. The Bell–Bloom magnetometer uses a single amplitude-modulated laser beam. A 589 nm laser illuminates the atoms, and the magnetic field is inferred from fluorescence collected at a photon detector. Magnetic resonance is detected at both  $D_1$  and  $D_2$  lines. A magnetic field sensitivity of  $150 \text{ pT}/\sqrt{\text{Hz}}$  is demonstrated at the  $D_1$  line. Considerable improvement can be expected by improving the power and wavelength stability of the laser, and increasing the involved sodium atoms with a bigger beam spot and optimized fluorescence-detecting optics.

A comparison of the setup with the mesospheric conditions is not straightforward. For atom magnetometry, the most relevant parameters are the number of the atoms involved in the measurement and the spin relaxation time. In the experiment the atom number is on the order of  $10^7$ , considering a detection volume of about  $1 \text{ cm}^3$ . The atom density in the mesosphere is only roughly  $3 \times 10^3 \text{ atoms/cm}^3$ . But the column density is roughly  $4 \times 10^{13} \text{ atoms/m}^2$ . Assuming a laser beam area of  $1 \text{ m}^2$ , the total number of sodium atoms involved will be on the order of  $10^{13}$ . The spin relaxation time is estimated to be 48 ms in the experiment condition, while at the mesosphere the spin relaxation time is about  $250 \text{ }\mu\text{s}$  [11]. However, for remote magnetometry with mesospheric sodium, the limiting parameter is the photon detection rate, which is calculated to be on the order of  $10^6 \text{ s}^{-1}$  providing a 20 W laser and  $1 \text{ m}^2$  telescope [11]. In the experiments, the photon detection rate is controlled to be the order of  $10^6 \text{ s}^{-1}$  as well to mimic the photon hungry condition of the remote mesospheric magnetometry.

## REFERENCES

1. D. Budker, D. F. Kimball, S. M. Rochester, V. V. Yashchuk, and M. Zolotarev, *Phys. Rev. A* **62**, 043403 (2000).
2. S. Groeger, G. Bison, J. L. Schenker, R. Wynands, and A. Weis, *Eur. Phys. J. D* **38**, 239 (2006).
3. I. K. Kominis, T. W. Kornack, J. C. Allred, and M. V. Romalis, *Nature* **422**, 596 (2003).
4. D. Budker and M. Romalis, *Nat. Phys.* **3**, 227 (2007).
5. V. Shah, S. Knappe, P. D. D. Schwindt, and J. Kitching, *Nat. Photonics* **1**, 649 (2007).
6. S. J. Seltzer, "Developments in alkali-metal atomic magnetometry," Ph.D. dissertation (Princeton University, 2008).
7. M. V. Romalis, *Phys. Rev. Lett.* **105**, 243001 (2010).
8. T. W. Hänsch, I. S. Shahin, and A. L. Schawlow, *Phys. Rev. Lett.* **27**, 707 (1971).
9. C. Y. She and J. R. Yu, *Appl. Opt.* **34**, 1063 (1995).
10. D. Suter, *Phys. Rev. A* **46**, 344 (1992).
11. J. M. Higbie, S. M. Rochester, B. Patton, R. Holzlohner, D. Bonaccini Calia, and D. Budker, *Proc. Natl. Acad. Sci. USA* **108**, 3522 (2011).
12. T. J. Kane, P. D. Hillman, C. A. Denman, M. Hart, R. P. Scott, M. E. Purucker, and S. J. Potashnik, "Laser remote magnetometry using mesospheric sodium," arXiv: 1610.05385 (2017).
13. W. E. Bell and A. L. Bloom, *Phys. Rev. Lett.* **6**, 280 (1961).
14. L. Zhang, Y. Yuan, Y. Liu, J. Wang, J. Hu, X. Lu, Y. Feng, and S. Zhu, *Appl. Opt.* **52**, 1636 (2013).
15. D. A. Steck, "Sodium  $D$  line data," report (Los Alamos National Laboratory, 2000), Vol. **124**.
16. A. T. Ramsey and L. W. Anderson, *Il Nuovo Cimento* (1955-1965) **32**, 1151 (1964).
17. W. Franzen, *Phys. Rev.* **115**, 850 (1959).
18. K. Jensen, N. Leefer, A. Jarmola, Y. Dumeige, V. M. Acosta, P. Kehayias, B. Patton, and D. Budker, *Phys. Rev. Lett.* **112**, 160802 (2014).
19. D. A. Steck, "Quantum and atom optics," revision 0.11.6, 2017, p. 360, <http://steck.us/teaching>.